First-principles study of hydrogen storage application of $Ti_3C_2T_x$ monolayer MXene

Yi Zhi Chu^{1,2}, Kah Chun Lau^{2*}

¹Department of Physics, Michigan Technological University, Houghton, MI 49931, USA
 ²Department of Physics and Astronomy, California State University, Northridge, CA 91330,
 USA

*Correspondence: <u>kahchun.lau@csun.edu</u>

Abstract

MXene, with its high aspect ratio and adjustable surface properties, has garnered significant attention in the realm of hydrogen storage research. For the first time, considering a ternary/quaternary mixed terminated MXene surface, the authors have investigated comprehensively the hydrogen storage potential of two-dimensional (2D) titanium carbide $Ti_3C_2T_x$ monolayer MXene using density functional theory (DFT). By considering mixed terminated surfaces, this study indicated the locally induced dipole due to the mixed termination is beneficial in facilitating hydrogen adsorption with stronger average adsorption energies than that of the uniform F-/O-/OH-/H-terminated surfaces. The authors estimated a compelling average H_2 surface adsorption energy on the ternary mixed termination and total surface storage capacity to be -0.14 eV/ H_2 and \sim 2 wt.% H_2 , which is comparable to that of the metal-organic frameworks (MOFs). This study also reveals the importance of the local surface chemistry effects on hydrogen adsorption.

Keywords: MXenes, Titanium carbide, Hydrogen storage materials, Hydrogen adsorption, Energy storage, Green energy, Density functional theory (DFT)

1. INTRODUCTION

Hydrogen fuel stands out as a promising long-term green energy solution, offering a clean alternative to conventional energy sources, particularly fossil fuels. Due to its highest gravimetric energy density (120 MJ/kg) among other fuels [1], coupled with the environmentally benign byproduct – water - upon consumption, hydrogen storage is crucial to the advancement of hydrogen fuel cell technology for transportation, stationary, and portable power application. Current conventional physical storage of hydrogen includes storing hydrogen in liquid (liquefaction) or gas phase (compression). However, both conventional storage methods demand extreme storage conditions rather than ambient conditions (*i.e.*, room temperature and atmospheric pressure). For instance, a high tank pressure of about 350-700 bar [2] is needed for gas storage of hydrogen while liquid hydrogen storage could only be achieved at cryogenic temperature owing to hydrogen's notably low boiling point (~20 K) [3]. These conditions inevitably pose safety risks and technological challenges that hinder their application for portable power applications of

hydrogen fuel. Thus, the search for higher efficiency whilst safer alternative methods has become extremely important [1, 4].

1 2

3

4

5

6

7

8

9

10

11

12

13

14

15

16

17

18

19

20

21

22

23

24

25

26

27

28

29

30

31

Among the alternative hydrogen storage methods, sorption-based storage, via physical or chemical adsorption on solid surfaces, provides an alternative safer storage method to address the challenges posed by extreme physical storage conditions [4]. In contrast to the conventional hydrogen storage methods, the sorption-based storage techniques utilize new materials to adsorb hydrogen gas molecules at relatively low pressure is promising. Novel materials like zeolites [5, 6] and metal-organic frameworks (MOFs) [7-9] are the representative materials that employ physisorption as a means to store hydrogen. MOFs, having high porosity and surface area [7], are ideal solid state-adsorbent materials for various applications, including hydrogen storage. Align with the United Nations' Sustainable Development Goal and the net zero target [10, 11], DOE has set a target for hydrogen fuel cells development to achieve a gravimetric density of 6.5 wt. %, with a milestone of 5.5 wt. % H₂ in 2025 [1] as one of the efforts to achieve higher energy efficiency improvement. The search for better-performance MOFs is generally compared to the benchmark MOF-5 due to its balanced performance between the volumetric (31.1 g-H₂/L) and gravimetric capacity (4.5 wt.%) [12]. In terms of the adsorption thermodynamics, Sagara et al. [13] have estimated that the hydrogen adsorption in MOF-5 to be in a broad range of energies from 0-7 kJ/mol at room temperature. Some of the MOFs demonstrated gravimetric capacity and adsorption enthalpy ranging from 1.5 to 2.5 wt.% and 6 to 10 kJ/mol respectively [14-16]. In addition, the estimated average adsorption energy of single-wall carbon nanotubes (SWCTs) with 0.8 nm diameter is about 8-9 kJ/mol. It is worth noting that the studies of MOFs' hydrogen adsorption capability have typically been carried out at temperatures as low as 77 K due to their low adsorption enthalpy [17].

Due to their appealing combination of properties such as a high aspect ratio [18, 19], MXenes have attracted immense theoretical and experimental research in various applications, such as battery systems [18], energy storage [20], and photocatalytic applications [21]. However, despite nearly a decade since its discovery [18], hydrogen storage application is one of the few areas where its potential has yet to be fully accessed. As the most studied MXenes to date, there were a few hydrogen storage application studies focused on $Ti_{n+1}C_nT_x$ (n = 1,2) in the literature. The first theoretical study of hydrogen storage application of pristine Ti_2C was conducted by Hu et al. [22], revealing a 3.4 wt.% H_2 uptake. Subsequently, considering uniformly O-/OH-/F-

terminated Ti_2C , Cheng et al. [23] found that $Ti_2C(OH)_2$ could uptake 2.7 wt.% H_2 . Experimentally, using incompletely etched Ti_2CT_x , Liu et al. [24] observed a hydrogen uptake of 8.8 wt.% at room temperature at 60 bar H_2 . Ghotia et al. [25] demonstrated the gravimetric density to be 10.47 wt.% at 77 K with 25 bar H_2 using $Ti_3C_2T_x$. Other theoretical studies of MXenes' hydrogen storage capacity have also shown promising results ranging from 5.3 to 9.0 wt.% H_2 [19, 22, 26, 27].

During the synthesis process, the highly reactive transition metal surface after etching results in a randomly distributed termination of surface functional groups (i.e., O, OH, F) on the MXenes surface, which is collectively expressed as T_x [28]. However, due to the complexity and computational cost of simulating mixed terminated surfaces, all of the above theoretical studies have considered either the bare MXenes [22, 26, 27, 29] or the homogeneously terminated surface with a single functional group [23, 29]. While these few MXenes have been studied for the purpose of hydrogen storage, the theoretical study of hydrogen storage application of Ti₃C₂T_x with mixed termination remains absent from the literature to date. As a baseline investigation, atomistic simulation of a mixed terminated MXene surface is crucial in basic understating of the MXene surface chemistry and can provide a more realistic model to bridge experimental characterizations [30]. In addition, the effect of various surface termination groups (e.g. O, OH, F, H, Cl) on the hydrogen adsorption and storage application of MXenes has also rarely been studied and remains elusive. Inspired by these, for the first time, considering various mixed terminated Ti₃C₂T_x surfaces adopted from Ref[31] the authors have systematically studied the local binding sites of the Ti₃C₂T_x monolayer on the hydrogen storage capability and estimated the hydrogen surface adsorption capacity. In this study, the authors have considered different MXene surfaces for H₂ adsorption, i.e., the bare Ti_3C_2 surface, the uniformly terminated $Ti_3C_2T_x$ surfaces ($T_x = F_2$, O_2 or OH_2), the ternary and quaternary mixed terminated surfaces $Ti_3C_2O_pOH_qF_rH_s(p+q+r+s=2)$.

2324

25

26

27

28

29

30

31

1

2

3

4

5

6

7

8

9

10

11

12

13

14

15

16

17

18

19

20

21

22

2. COMPUTATIONAL DETAILS

To model the 2D Ti₃C₂T_x structures, first-principles density functional theory (DFT) was employed as implemented in Vienna Ab initio Simulation Package (VASP) [32, 33] for the spin-polarized electronic structure calculations. The projector-augmented-wave (PAW) pseudopotential method, together with the generalized gradient approximation (GGA) and the Perdew–Burke–Ernzerhof (PBE) exchange-correlation functional were used to represent the exchange-correlation effects in the DFT simulation [34]. The kinetic energy cutoff for the plane-

1 wave basis was set at 500 eV. For the structural optimization and electronic calculations, the

Brillouin zone was sampled using a Γ -centered grid of (3 \times 3 \times 1). The electronic self-consistent

cycle energy convergence was set at $1 \times 10^{-5} eV$ and the residual force on each atom is less than

 $1 \times 10^{-4} \, eV/\dot{A}$. The van der Waals interaction was included in all calculations using the semi-

empirical approach of Grimme (DFT-D3) [35]. A vacuum slab of at least 15 Å along the z-axis

was implemented for the monolayer structure calculations to avoid spurious interactions between

7 mirror images in simulation. The hydrogen surface adsorption energy is calculated as:

$$E_{adsorption/H_2} = \frac{(E_{Ti_3C_2T_x} - E_{Ti_3C_2} - nE_{H_2})}{n}$$
 (1)

9 where $E_{adsorption/H_2}$, $E_{Ti_3C_2T_x}$, $E_{Ti_3C_2}$, and E_{H_2} are the adsorption energy per H₂, total energy of

 $Ti_3C_2T_x$, total energy of the bare Ti_3C_2 structure, and the total energy of the hydrogen molecule.

11 The number of adsorbed H_2 are denoted by n.

To estimate the hydrogen storage capacity of various Ti_3C_2 monolayer derivatives (Section 3.1-3.3) that mainly determined by H_2 adsorption on surfaces, instead, the authors use hydrogen

surface adsorption capacity (ω_{H_2}) as an approximation, with the weight capacity is calculated as

15 [23]:

2

3

4

5

6

10

12

13

14

16

18

20

21

$$\omega_{H_2} = \frac{M_{H_2}}{M_{Ti_3C_2T_x} + M_{H_2}} \times 100\%$$
 (2)

where ω_{H_2} is the weight capacity, M_{H_2} and $M_{Ti_3C_2T_x}$ are the molecular masses of $Ti_3C_2T_x$ and H_2

respectively. All atomic structures and charge densities are visualized using the open-sourced

visualization software VESTA [36].

2223

24

25

26

27

28

29

30

3. RESULTS AND DISCUSSIONS

3.1. Hydrogen adsorption on a bare Ti₃C₂

The pristine Ti_3C_2 surface is highly reactive and could facilitate hydrogen adsorption. To study the hydrogen surface adsorption capability of a bare Ti_3C_2 , the authors first investigate the favorable adsorption site for H_2 adsorption. A $5 \times 5 \times 1$ supercell of Ti_3C_2 was constructed corresponding to a total of 25 adsorption sites per surface. The high-symmetry adsorption sites are the Top (on top of the outer layer Ti atoms), face-centered cubic (FCC) (on top of the middle layer

Ti atoms in the hollow site), and hexagonal close-packed (HCP) (on top of the C atoms in the hollow site) sites, as depicted in Figure 1.(a). Interestingly, without any surface functionalization and regardless of the adsorption sites, the H₂ molecules would dissociate into H atoms (Figure 1.(b)) and bind strongly with the Ti₃C₂ surface forming Ti-H bonds at the FCC site with an average adsorption energy of -1.2 eV/H₂, similar to the H₂ adsorption on a bare Ti₂C surface [22-24]. Such strong surface adsorption is attributed to the chemisorption, where an H-termination-like surface is formed, with comparable adsorption energy to that of the formation energy per adatom of a fully H-functionalized Ti₃C₂ surface (see Figure S1). Considering the 100% H-termination on the FCC sites, the estimated hydrogen storage capacity is calculated to be 1.2 wt. % H.

1

2

3

4

5

6

7

8

9

10

11

12

13

14

15

16

17

18

19

20

21

22

23

24

25

26

27

28

29

Due to the dissociation of H₂ molecule and the nature of strong chemisorption that form Ti-H bonds, the bare Ti₃C₂ surface would not be helpful for a reversible hydrogen uptake in hydrogen storage application especially at ambient condition. The dissociation of the H₂ molecules and subsequent chemisorption of the H atoms on the MXene surface, however, provides a new insight into considering H-termination as a functional group which has rarely been studied in the past. Complimentary to this study, the authors have also systematically studied the thermodynamic stability of the H-terminated Ti₃C₂T_x by calculating the formation energies when transitioning from a bare to a full H-termination surface (Figure S1) and found that a constant formation energy of -1.26 eV/H atom was observed when varying the H percent coverage. The favorable adsorption site for H atoms is the FCC site which explains the chemisorption of the dissociated H atoms formation on the FCC site upon H₂ adsorption. The study of H₂ adsorption on the uniformly H-terminated surface is thus also considered in the following section. To examine the interaction between the Ti₃C₂ surface and hydrogen atoms/molecules, the authors have calculated the charged density difference and performed the Bader charge analysis [37, 38]. The Bader charge analysis (Figure 2) shows -0.61e of Bader charge on the adsorbed hydrogen atom, and an extra +0.14e and +0.06e of Bader charge on the nearest Ti and C atoms respectively, further confirming a strong bonding of H adatom to the surface. This explains the relatively large adsorption energy is essentially attributed to the formation of strong chemical bonds of hydrogen atoms on Ti sites (i.e. Ti-H bonds) on the surface upon chemisorption.

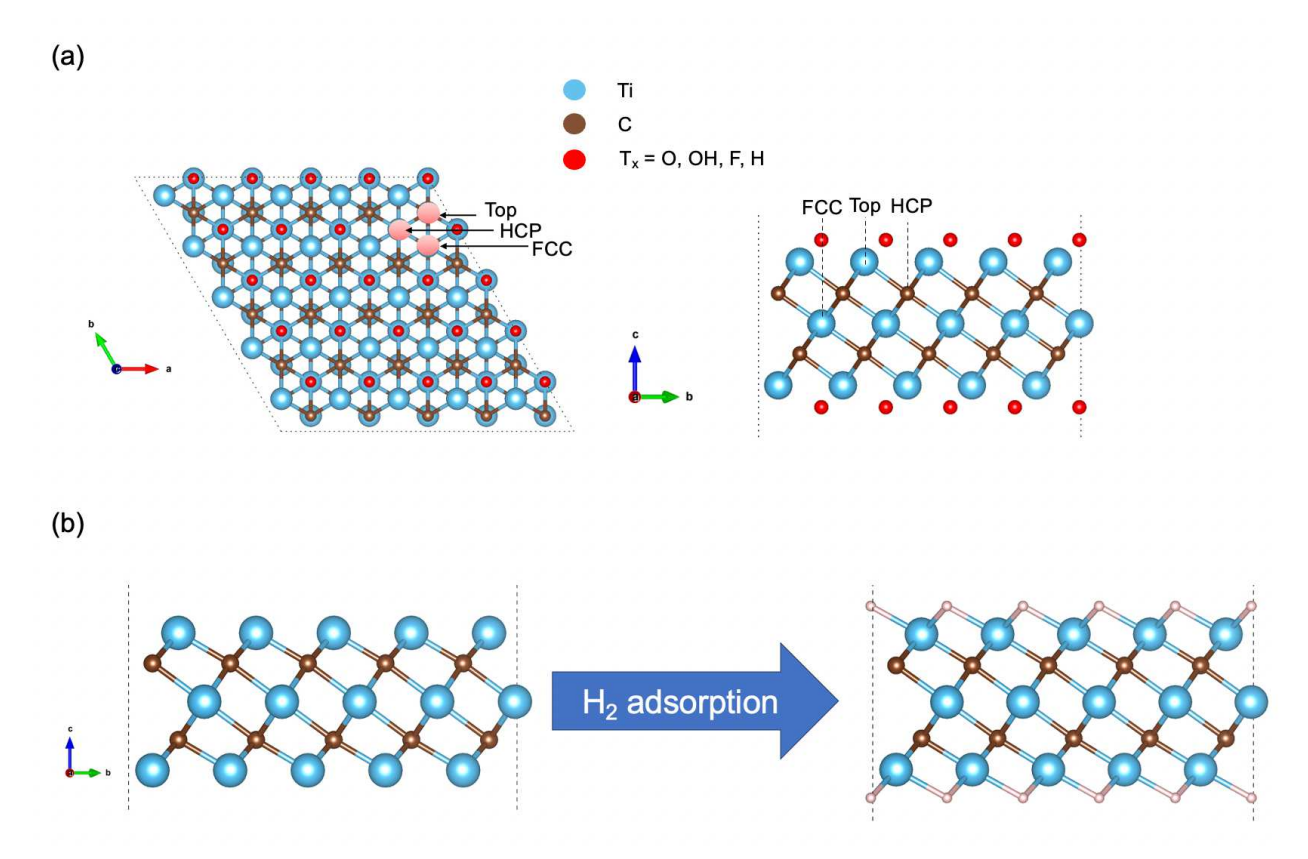
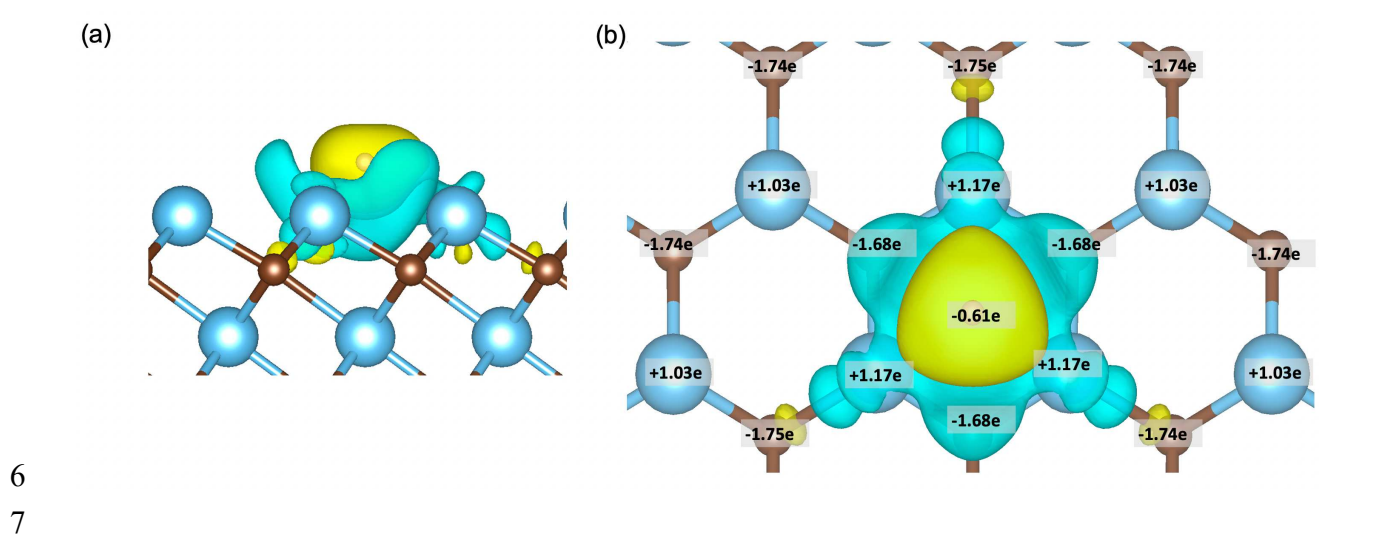


Figure 1. (a) Adsorption sites for hydrogen molecules as inspected from the top and side view. (b) The dissociation of H_2 molecule into the formation of Ti-H bond upon H_2 adsorption on a bare Ti_3C_2 surface.



- Figure 2. (a) Side view and (b) top view of the charge density difference and Bader charge of the
- 2 H-terminated Ti₃C₂. The yellow and cyan region represents charge accumulation and depletion
- 3 respectively. Color code for atoms: Blue: Ti, Brown: C, Pink: H.

5 Table 1: Theoretical hydrogen storage capacity of physisorption-based material.

Materials	Average adsorption	Total H/H ₂ storage	Reference
	energy (eV/H or eV/ H_2)	capacity (wt.%)	
MOFs	-0.06-0.10	1.5-2.5	[14-16]
Bare Ti ₃ C ₂	-1.26	1.2#	This work
Bare Ti ₂ C	-5.03	8.61,2	[22]
Bare Cr ₂ C	-0.96	$7.6^{1,2}$	[26]
Bare Ti ₂ N	-3.63	$8.6^{1.2}$	[29]
Bare Sc ₂ C	-4.70	9.01,2	[27]
Ti ₂ CO ₂	-0.14	5.3^{2}	
Ti_2CF_2	-0.13	5.2^{2}	[23]
$Ti_2C(OH)_2$	-0.14	5.3^{2}	
Ti_2NO_2	-0.14	5.42	
Ti_2NF_2	-0.14	5.2^{2}	[29]
$Ti_2N(OH)_2$	-0.15	5.3^{2}	
Ti ₃ C ₂ O ₂	-0.10	2.0	
$Ti_3C_2F_2$	-0.08	2.0	This work
$Ti_3C_2(OH)_2$	-0.10	1.9	
$Ti_3C_2H_2$	-0.11	$3.4^{1,*}$	
$Ti_3C_2O_p(OH)_qF_r$	-0.14	1.9	This work
(p+q+r=2)	-0.14	1.7	THIS WOLK

^{6 #}Irreversible chemisorbed hydrogen atoms, a model to be considered as Ti₃C₂H₂

^{7 &}lt;sup>1</sup>Including irreversible chemisorbed hydrogen atoms.

^{8 &}lt;sup>2</sup>Two layers of physisorbed hydrogen molecules.

^{9 *}H₂ adsorption on the H-chemisorbed Ti₃C₂

3.2. Hydrogen adsorption on a uniformly terminated Ti₃C₂T_x

The next model to be considered is the homogenously terminated Ti₃C₂T_x, i.e., Ti₃C₂ uniformly terminated with the O/OH/F/H functional group adatoms. Upon termination, taking the bare Ti₃C₂ as the reference, the favorable adsorption sites on the 2D Ti₃C₂T_x were determined. To determine the most favorable adsorption sites under full coverage of H₂, these three adsorption sites were fully populated with H₂ (i.e., 100% H₂ coverage) (Figure 3. a, b), and their adsorption energies were subsequently calculated and summarized in Table 1. As opposed to the H₂ adsorption on the bare Ti₃C₂ where the occurrence of H₂ dissociation into Ti-H bond formation was observed, whereas upon the adsorption on the functionalized Ti₃C₂ surface, H₂ molecules remain intact with no decomposition. In addition, the formerly most reactive FCC site now exhibits the weakest average adsorption energy, regardless of the termination species (see Table S1). The favorable hydrogen adsorption site for the uniformly terminated Ti₃C₂T_x surface can be explained with the favorable functionalization site study. Since the FCC site is the most reactive site for both the interaction between the functional group adatoms, (including hydrogen) with the bare Ti₃C₂ sheet, with all the FCC sites now being functionalized, the H₂ adsorption is now significantly weakened. Hence, further interaction among the surface adsorbed H₂ molecules and functionalized Ti₃C₂ surface would not break the H₂ bond.

In terms of average adsorption energy, the HCP and FCC sites demonstrated a comparable strength for H_2 physisorption with a subtle difference of \sim 1-10 meV/ H_2 . The average physisorption energy ranges from \sim -0.08 to -0.10 eV/ H_2 with varying termination species, wherein OH termination and F termination have the strongest and weakest average adsorption energy respectively. Note that, the average physisorption energies of H_2 on uniformly terminated $Ti_3C_2T_x$ are at least one order of magnitude lower than that of the H_2 chemisorption on the bare Ti_3C_2 . For the bare Ti_3C_2 , it would be more suitable for high-temperature hydrogen storage applications due to strong chemisorption and chemical dissociation of H_2 on Ti-sites (Section 3.1). Based on Eq. 2, the estimated hydrogen surface storage capacities due to physisorbed H_2 are approximately 2.0 wt. % H_2 for uniform F-/O-/OH-/H-terminated Ti_3C_2 . In particular, the H-terminated Ti_3C_2 has notably higher hydrogen storage capacity, considering the non-reversible terminated H adatom on the $Ti_3C_2H_2$ surface, the hydrogen surface adsorption capacity (ω_{H_2}) reaches \sim 3.4 wt. % with 2.3 wt. % is attributed to physisorbed H_2 and 1.2 wt. % is due to chemisorbed hydrogen (Figure 1. b). In general, H_2 adsorption on the uniformly terminated $Ti_3C_2T_x$ exhibit a weak adsorbate/adsorbent

interaction, indicating a significantly weak bonding among the adsorbent/adsorbate in 1 physisorption regime as opposed to the case of chemisorbed Ti₃C₂H₂ (Section 3.1). Interestingly, 2 3 for single H₂ adsorption on Ti₃C₂O₂ (Figure 3. c), a significant Bader charge of +0.84e is found on the hydrogen molecules and an extra of -0.07e and -0.02e respectively on the nearest and second 4 5 nearest terminated oxygen atoms. A relatively subtle change in Bader charges was found for H₂ adsorption on Ti₃C₂OH₂ (Figure 3. d). For Ti₃C₂F₂ and Ti₃C₂H₂ (see Figure S2), the adsorption of 6 7 single H₂ would not change the Bader charge significantly, suggesting a very weak interaction of 8 the surfaces with H_2 on the uniformly terminated $Ti_3C_2T_x$ surfaces.

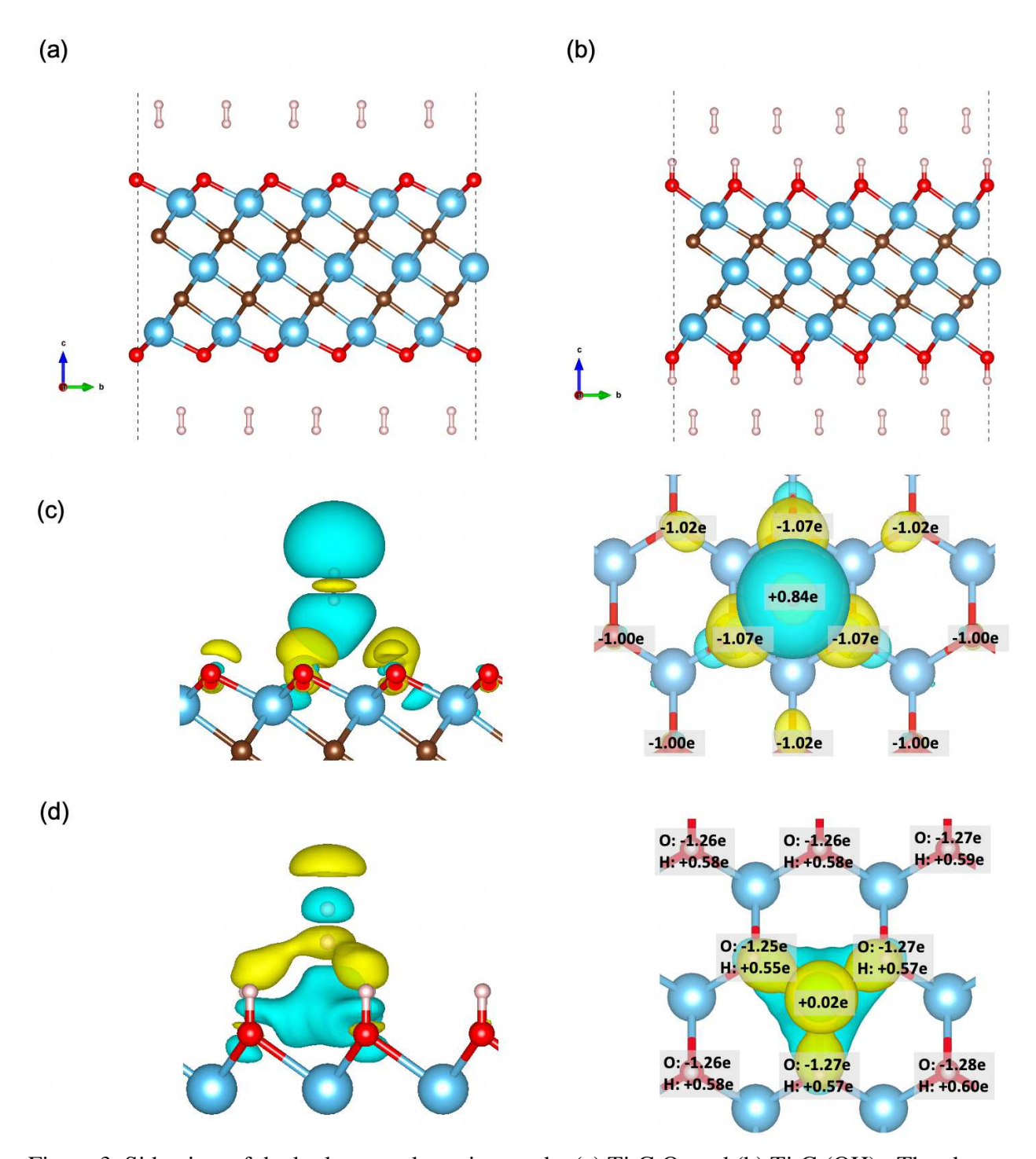


Figure 3. Side view of the hydrogen adsorption on the (a) $Ti_3C_2O_2$ and (b) $Ti_3C_2(OH)_2$. The charge density difference and Bader charge of the H_2 adsorbed on (c) $Ti_3C_2O_2$ and (d) $Ti_3C_2(OH)_2$. The yellow and cyan region represents charge accumulation and depletion respectively. Color code for atoms: Blue: Ti, Brown: C, Pink: H, Red: O.

3.3. Hydrogen adsorption on mixed terminated Ti₃C₂T_x

3.3.1. Ternary mixed terminated $Ti_3C_2T_x$

1

2

24

25

26

27

28

29

30

31

3 To study a more realistic model of Ti₃C₂T_x for H₂ adsorption study, a single-layer Ti₃C₂T_x 4 sheet terminated with the ternary mixed termination of O, OH, and F functional groups (i.e., 5 $Ti_3C_2T_x$, where T_x is represented by $O_p(OH)_qF_r$ and p+q+r=2.0) which based on Ref [31], are 6 considered (Figure 4). Based on a recent work by Chu et. al. [31], the thermodynamic stability and 7 electronic properties of Ti₃C₂T_x etched with different HF concentrations, by considering various 8 T_x stoichiometry has been studied. Similar to the 100% H₂ adsorption study in Sect. 3.2, 12 9 different structures reported from Ref [31] with different stoichiometries were populated with 10 hydrogen molecules, and the average H₂ adsorption energies were subsequently calculated and 11 summarized in Table 1 and Table S2. The mixed terminated surfaces in general exhibit 12 physisorption with H₂ molecules (Figure 4), with average adsorption energy in the range of ~-0.11 13 to -0.14 eV/H₂, which is relatively higher than that of the uniformly terminated surfaces discussed 14 in Sect. 3.2. The authors believe that the locally induced dipole due to the local imbalanced charges 15 of OH, O and F terminating group as a result of the mixed termination surface revealed in Ref [31], 16 could have a substantial contribution to molecular hydrogen adsorption. Inspired by this finding 17 [31], the authors have also systematically examined the strength of molecular hydrogen adsorption 18 on individual adsorption sites. In this regard, instead of considering 100% H₂ coverage adsorption, 19 the authors only populate each individual binding site with H₂. The possible hydrogen adsorption 20 sites on the mixed terminated surface are similar to the previous section, however, due to the 21 permutation of O/OH/F terminating species on these favorable sites, there are 10 possible local 22 distributions to be considered (see Figure 4. c), known as O_O_O, OH_OH_OH, F_F_F, O_O_OH, 23 O_OH_OH, O_O_F, O_F_F, F_F_OH, F_OH_OH, and F_O_OH.

By taking the average of the adsorption energies of H_2 adsorption on each individual site on these 12 surfaces with different terminations and stoichiometries, a site-dependent H_2 adsorption energy strength is highlighted in Figure 5. Interestingly, the weakest H_2 adsorptions are found to correspond to the adsorption sites terminated with the same species of the functional group adatom (O_O_O/OH_OH_OH/F_F_F), with an average adsorption energy of \sim -0.08 to -0.10 eV/ H_2 , which is consistent with the H_2 adsorption energy strength on the uniformly terminated surface discussed in Section 3.2. As expected, due to the locally induced dipole formed at the adsorption site, the O_OH_OH site is found to be the strongest binding site (*i.e.*, \sim -0.16 eV/ H_2) for

 H_2 adsorption, demonstrating an average adsorption energy of which is twice as much as the binding sites terminated with the homogenous species (Section 3.2). In general, the presence of two OH groups in binding site (Figure 5) would result in the average adsorption energies larger than \sim -0.12 eV/ H_2 . As demonstrated in the charge density difference and Bader charge analysis (Figure 6), the adsorption of the H_2 molecule on the surface would result in the polarization of the physisorbed H_2 molecule, where charges (-0.08e) are accumulated on the hydrogen atom facing further away from the surface while depleted on the other end of hydrogen atom closer to the surface (+0.08e). Consequently, the physisorbed H_2 would also induce the charge transfer (about 0.08e) among the hydroxyl group atoms (O-H) on binding site. Meanwhile, the effect of the physisorbed H_2 on the F and O termination adatoms on mixed terminated $Ti_3C_2T_x$ surface is minimal, with the Bader charge remaining nearly unchanged before and after the H_2 physisorption.

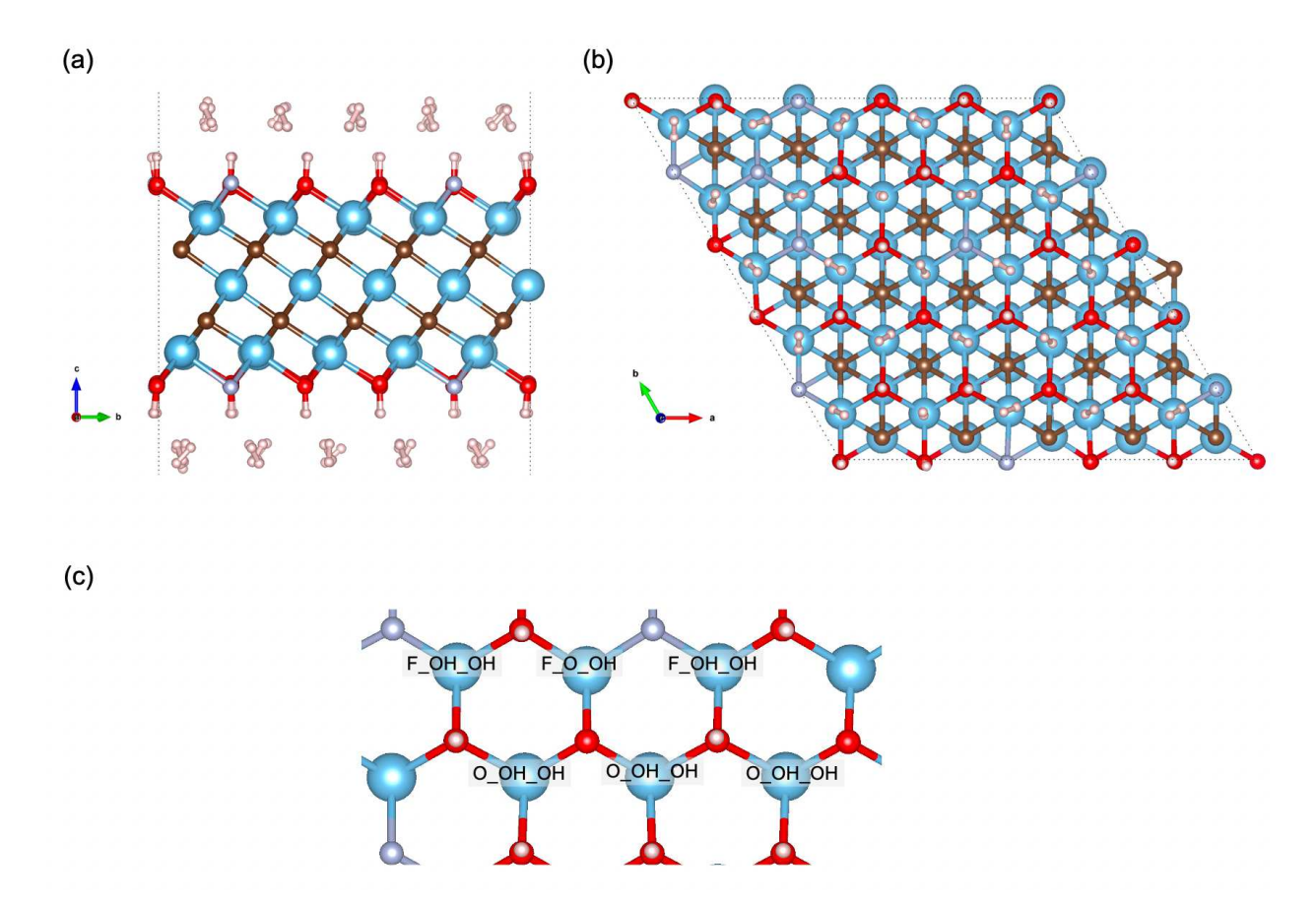


Figure 4. (a) Side view and (b) top view of ternary mixed $Ti_3C_2T_x$ with 100% coverage of H_2 adsorption. (c) The nomenclature of the hydrogen adsorption sites on a ternary mixed terminated $Ti_3C_2T_x$ surface. Color code for atoms: Blue: Ti, Brown: C, Pink: H, Red: O, Purple: F.



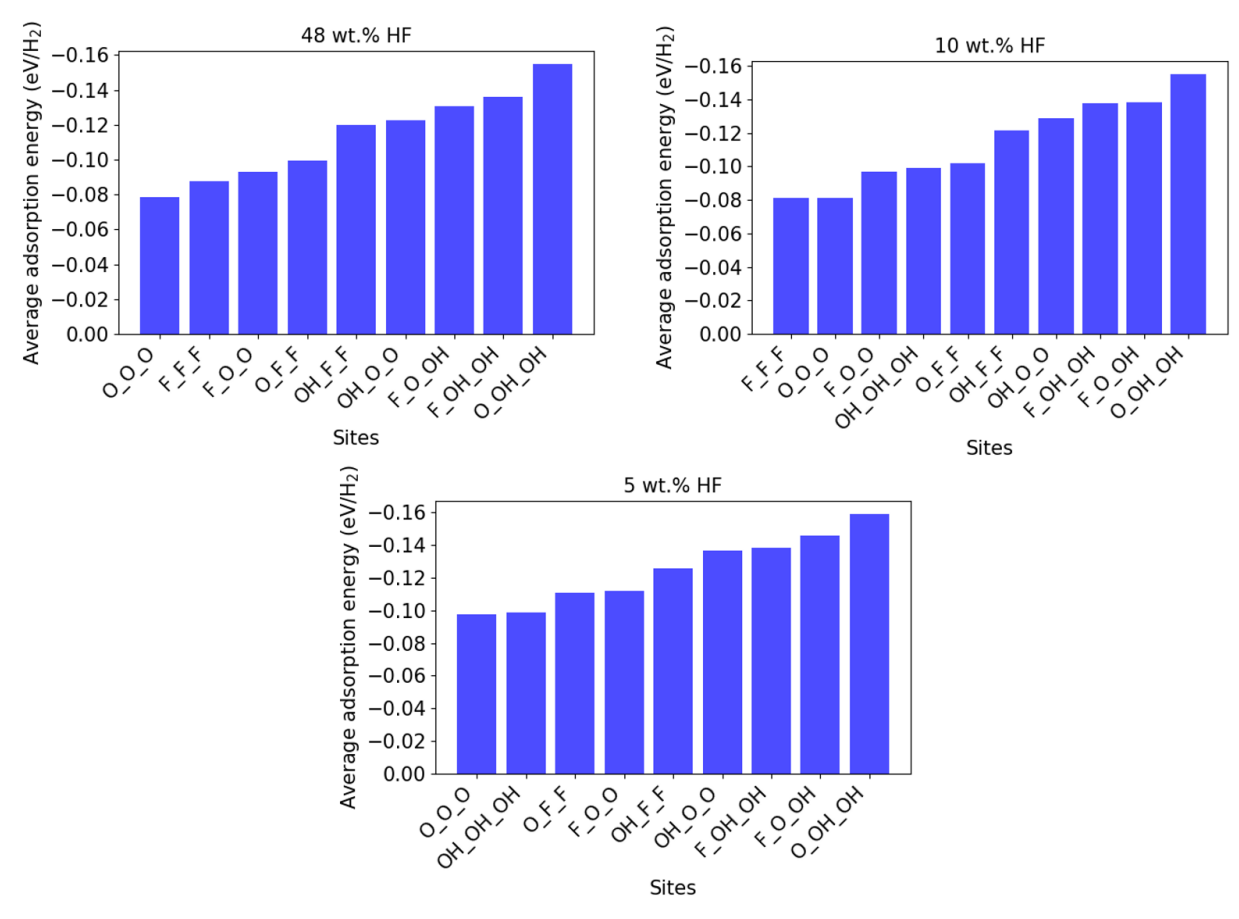


Figure 5: Site-dependent average adsorption energy of hydrogen on 48 wt. %,10 wt. % and 5 wt. % HF etched surfaces.



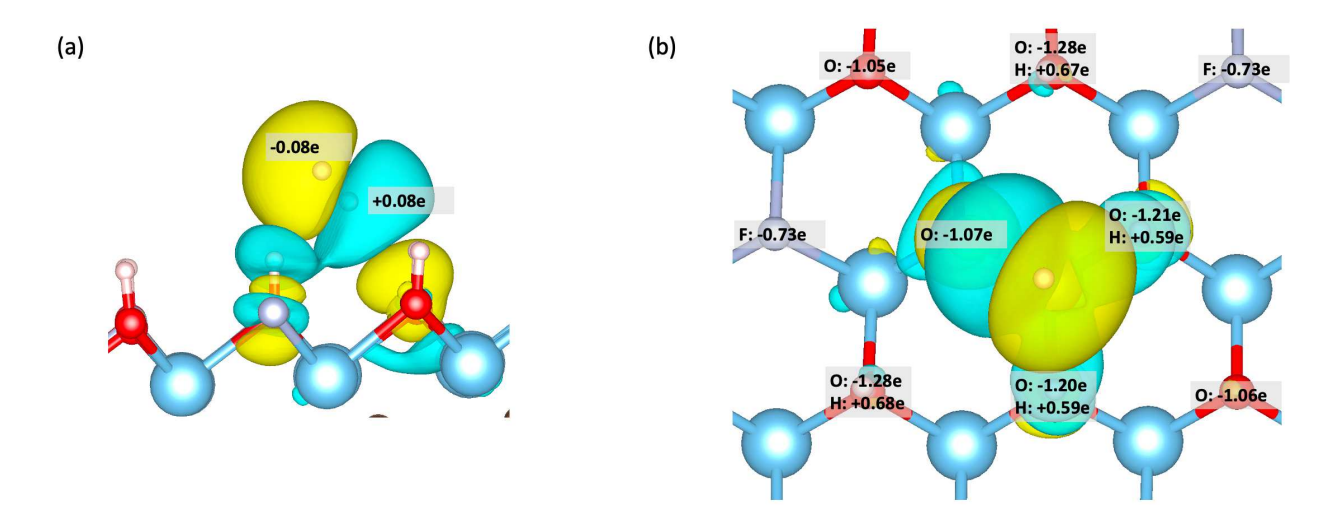


Figure 6. (a) Side view and (b) top view of the charge density difference and Bader charge of the single H₂ adsorbed on ternary mixed terminated Ti₃C₂T_x. The yellow and cyan region represents charge accumulation and depletion respectively. Color code for atoms: Blue: Ti, Brown: C, Pink: H, Red: O, Purple: F.

5

6

7

8

9

10

11

12

13

14

15

16

17

18

19

20

From Table S2 and Figure 5, it was found that the greater number of the three most favorable adsorption sites (i.e., O_OH_OH, F_OH_OH, and F_O_OH) would be beneficial for the overall H₂ adsorption regardless of the HF concentration. Thus, to enhance the hydrogen adsorption strength on a ternary mixed terminated Ti₃C₂T_x, the surface with as many OH mixture sites or OH-rich ternary mixed terminated Ti₃C₂T_x surfaces (e.g. O_{0.24}OH_{1.28}F_{0.48} and O_{0.48}OH_{1.04}F_{0.48} in Table S2) would be useful. As highlighted in Table S2, the subtle difference of ~20 meV/H₂ in terms of the average H₂ adsorption energy between the 48 wt. % HF etched surface and the 5 wt. % HF etched surface could be explained based on the available number of OH-mixed sites on the Ti₃C₂T_x surface. Thus, a least acidic environment (i.e., small wt.% HF) would result in a relatively higher OH to F ratio, which is a synthesis condition beneficial for hydrogen adsorption application. The estimated average lower bound of hydrogen storage capacity of a mixed terminated Ti₃C₂T_x is approximately 2.0 wt. % H₂. It is worth mentioning that in all the above models (i.e., bare, homogeneously, and mixed terminated Ti₃C₂) considered for the hydrogen adsorption study, the adsorption energies and capacities are comparable to some of the most promising physisorption material such as MOF [14-16] (Table 1) and some of the MXenes, suggesting that Ti₃C₂T_x monolayers could be a promising H₂ adsorption material.

2122

23

24

25

26

27

28

29

30

3.3.1. Quaternary mixed terminated Ti₃C₂T_x

Complimentary to the study of ternary terminated $Ti_3C_2T_x$, by considering hydrogen as a possible termination species, the authors have also investigated the hydrogen adsorption properties of the quaternary mixed terminated $Ti_3C_2T_x$. From Figure S3, the increase in H adatoms ratio on the surface coverage as the dominant terminating group in quaternary mixed terminated $Ti_3C_2T_x$ is found to be thermodynamic less favorable. Thus, to make a concise discussion on the H_2 adsorption on quaternary mixed terminated $Ti_3C_2T_x$ with T_x consisting of O, OH, F, and H terminating group, the authors shall only focus on quaternary mixed terminated $Ti_3C_2T_x$ with half of the OH

termination group being randomly substituted with H adatoms, leading to a stoichiometry $T_x = O_{0.24}OH_{0.64}F_{0.48}H_{0.64}$ (Figure S3).

Following the same methodology, the authors have subsequently calculated the total hydrogen storage capacity and its average H_2 adsorption energies (see Table S3). The trend of the site-dependent H_2 adsorption strength is consistent with Figure 5, where, despite having a large amount of surface OH species being substituted by H adatoms, the local sites dominated with OH species (mixed with other species) still exhibit relatively larger H_2 adsorption energy. For this quaternary mixed terminated $T_{13}C_2T_x$, i.e. $T_x = O_{0.24}OH_{0.64}F_{0.48}H_{0.64}$, the estimated hydrogen surface adsorption capacity (ω_{H_2}) is about 2.4 wt. % H_2 , comparable to some of the most promising physisorption material such as MOF [14-16] (Table 1), and is between the upper bound of the fully H-chemisorbed surface (3.4 wt. %) and the H-termination free ternary mixed terminated $T_{13}C_2T_x$, surfaces (1.9 wt. % in Table S2). In theory, tuning the surface termination by H-functionalization through H adatoms could eventually increase the overall H_2 surface adsorption capacity (ω_{H_2}), which attributed to surface-terminated H adatoms. However, the irreversible hydrogen stored in such systems would eventually require a significantly larger amount of thermal energy to break the strong T_1 -H bonding, i.e., at high temperatures to release the chemisorbed hydrogen, and might compromise the efficiency of hydrogen uptake of these $T_{13}C_2T_x$ surfaces.

4. CONCLUSION

As a baseline study, the authors have conducted a comprehensive theoretical investigation into the hydrogen storage capabilities based on H_2 surface adsorption capacity (ω_{H_2}) as an approximation on several types of Ti_3C_2 monolayer: the bare Ti_3C_2 structure, the uniformly terminated $Ti_3C_2T_x$, ternary and quaternary mixed terminated $Ti_3C_2T_x$. Based on DFT calculations, this research underscores the substantial influence of surface termination on the interaction between hydrogen and the MXene surface.

Without any surface termination, the highly reactive bare Ti_3C_2 surface would dissociate the H_2 bond and subsequently form a strong Ti-H bond with a relatively strong binding energy of $1.2~eV/H_2$. The strong H binding energy, attributed to the chemisorption, would require a substantial amount of thermal energy to desorb the stored hydrogens. Upon uniform/mixed surface termination, the hydrogen molecules physiosorbed on the $Ti_3C_2T_x$ surface with average adsorption energy ranging -0.08 to $-0.14~eV/H_2$ without the dissociation of H_2 bonds.

From DFT prediction, the authors have investigated the effects of the mixed terminating group on the interaction of molecular hydrogen with the MXene surface. From DFT calculations, an enhanced H₂ adsorption energy in the case of ternary/quarternary mixed terminated Ti₃C₂T_x surfaces is observed, in contrast to the uniformly terminated Ti₃C₂T_x surface. From electronic properties analysis, the enhanced H₂ adsorption energy can be attributed to the locally induced dipoles resulting from local imbalanced charges present on the mixed-termination surfaces. Among these quaternary and ternary mixed-termination Ti₃C₂T_x surfaces, the local adsorption sites dominated with OH species (mixed with other species) generally exhibit relatively larger H₂ adsorption energy and is facilitating the hydrogen physisorption capability. The locally induced dipole because of a mixed terminated MXene surface has been proven to render unique surface chemistry, as indicated in the difference in the adsorption energy and the Bader charge analysis. The authors believe that this work highlights the importance of constructing a more realistic model of MXene surface (i.e., mixed terminated surface) to capture the unique microscopic features of local electronic effects which is otherwise absent if considering a highly idealized surface model (e.g., uniform terminated surfaces). The inhomogeneous/imbalanced charge distribution on the mixed terminated surface of MXene could serve as a reactive site not only for hydrogen storage study but also for other important applications in surface chemistry (e.g. catalysis and gas adsorption).

Based on H₂ adsorption on these Ti₃C₂T_x surfaces, the findings suggest these MXene surfaces could possibly be a promising hydrogen storage nanomaterial based on physisorption, especially for low-temperature storage of H₂. From the calculated H₂ surface adsorption capacity (ω_{H_2}) , a minimum storage capacity of approximately 2 wt.% H₂, with an average H₂ adsorption energy of approximately -0.14 eV/H₂ comparable to that of MOFs is found. This falls into the desirable range of hydrogen binding energy of 10-20 kJ/mol (0.10-0.20 eV/H₂) for practical application [19]. The comparable adsorption energy of hydrogen with MOFs suggested that such hydrogen storage system is suitable for low temperature application but would be unfeasible for ambient temperature storage of H₂. Nevertheless, MXenes is well-known nanomaterials due to their high aspect ratio and tunable surfaces, slit-shape mass transport channels which suggests that MXenes could be a promising candidate as adsorbent for sorption-based hydrogen storage system. Thus, to go beyond the influence of MXene monolayer surfaces which is a focus of this work, future investigation on the effects of H₂ adsorption on terminating edges, and H₂ confinement within bulk Ti₃C₂T_x interlayers might be worthwhile. Meanwhile, to further functionalize the surface properties, metal decorated MXene surfaces could possibly serve as a potential route to the enhancement of hydrogen adsorption and storage.

1718

19

1

2

3

4

5

6

7

8

9

10

11

12

13

14

15

16

ACKNOWLEDGEMENT

- 20 The contribution of computing resources through NSF-MRI: NSF OAC-2117956 is acknowledged.
- 21 The authors acknowledge the support of the U.S. Department of Energy, Office of Science, Office
- of Basic Energy Sciences, Division of Materials Sciences and Engineering. The authors would like
- 23 to extend their gratitude to Dr. Megan Hoover and Dr. Patrick Ward for their valuable and
- 24 insightful discussion and comments in the production of this paper.

2526

REFERENCES

2829

30

27

1. DOE, Target Explanation Document: Onboard Hydrogen Storage for Light-Duty Fuel Cell Vehicles 2017.

- Hua, T.Q., et al. (2011). Technical assessment of compressed hydrogen storage tank systems for automotive applications. International Journal of Hydrogen Energy. **36**(4)3037-3049.
- 4 3. Rossini, F.D. (1970). A Report on the International Practical Temperature Scale of 1968. Pure and applied chemistry. **22**(3)555-570.
- 4. Le, T.T., et al. (2023). Fueling the future: A comprehensive review of hydrogen energy systems and their challenges. International Journal of Hydrogen Energy.
- 8 5. Lee, S.-Y., et al. (2022). Recent Progress Using Solid-State Materials for Hydrogen Storage: A Short Review. Processes. 10(2)304.
- Sun, Y., et al. (2021). Fingerprinting diverse nanoporous materials for optimal hydrogen storage conditions using meta-learning. Science Advances. 7(30)eabg3983.
- 7. Zhao, D., et al. (2022). *Porous metal–organic frameworks for hydrogen storage*. Chemical Communications. **58**(79)11059-11078.
- Shet, S.P., et al. (2021). A review on current trends in potential use of metal-organic framework for hydrogen storage. International Journal of Hydrogen Energy. **46**(21)11782-11803.
- 9. Zeleňák, V. and I. Saldan. (2021). Factors Affecting Hydrogen Adsorption in Metal-Organic Frameworks: A Short Review. Nanomaterials. 11(7)1638.
- 19 10. UN. Department of Economic and Social Affairs Sustainable Development. Available from: https://sdgs.un.org.
- 21 11. UN. For a livable climate: Net-zero commitments must be backed by credible action.
 22 Available from: https://www.un.org/en/climatechange/net-zero-coalition.
- 23 12. Ahmed, A., et al. (2017). *Balancing gravimetric and volumetric hydrogen density in MOFs*. Energy & environmental science. **10**(11)2459-2471.
- 25 13. Sagara, T., J. Klassen, and E. Ganz. (2004). *Computational study of hydrogen binding by metal-organic framework-5*. The Journal of chemical physics. **121**(24)12543-12547.
- 27 14. Singh, R., A. Altaee, and S. Gautam. (2020). *Nanomaterials in the advancement of hydrogen energy storage*. Heliyon. **6**(7)e04487.
- 29 15. Latroche, M., et al. (2006). *Hydrogen Storage in the Giant-Pore Metal-Organic Frameworks MIL-100 and MIL-101*. Angewandte Chemie. **118**(48)8407-8411.
- 31 16. Rowsell, J.L.C. and O.M. Yaghi. (2006). Effects of Functionalization, Catenation, and Variation of the Metal Oxide and Organic Linking Units on the Low-Pressure Hydrogen Adsorption Properties of Metal—Organic Frameworks. Journal of the American Chemical Society. 128(4)1304-1315.
- 35 17. Germain, J., J.M.J. Fréchet, and F. Svec. (2009). Nanoporous Polymers for Hydrogen Storage. Small. 5(10)1098-1111.
- 37 18. Gogotsi, Y. and B. Anasori. (2019). *The Rise of MXenes*. ACS Nano. **13**(8)8491-8494.
- 38 19. Kumar, P., et al. (2021). *MXenes: Emerging 2D materials for hydrogen storage*. Nano Energy. **85**105989.
- 40 20. Li, X., et al. (2022). *MXene chemistry, electrochemistry and energy storage applications*. Nature Reviews Chemistry. **6**(6)389-404.
- 42 21. Murali, G., et al. (2022). A Review on MXene Synthesis, Stability, and Photocatalytic Applications. ACS Nano. 16(9)13370-13429.
- Hu, Q., et al. (2013). *MXene: A New Family of Promising Hydrogen Storage Medium*. The Journal of Physical Chemistry A. **117**(51)14253-14260.

- 1 23. Cheng, Y., et al. (2022). The effect of functional groups (O, F, or OH) on reversible hydrogen storage properties of Ti2X (X=C or N) monolayer. International Journal of Hydrogen Energy. 47(67)28969-28977.
- 4 24. Liu, S., et al. (2021). *Hydrogen storage in incompletely etched multilayer Ti2CTx at room temperature*. Nature Nanotechnology. **16**(3)331-336.
- 6 25. Ghotia, S., et al. (2023). *Multilayered Ti3C2Tx MXenes: A prominent materials for hydrogen storage*. International Journal of Hydrogen Energy.
- 8 26. Yadav, A., et al. (2016). Study of 2D MXene Cr2C material for hydrogen storage using density functional theory. Applied Surface Science. **389**88-95.
- Hu, Q., et al. (2014). Two-dimensional Sc2C: A reversible and high-capacity hydrogen storage material predicted by first-principles calculations. International Journal of Hydrogen Energy. **39**(20)10606-10612.
- Wang, X., et al. (2015). Atomic-Scale Recognition of Surface Structure and Intercalation
 Mechanism of Ti3C2X. Journal of the American Chemical Society. 137(7)2715-2721.
- Li, Y., et al. (2019). Reversible hydrogen storage behaviors of Ti2N MXenes predicted by first-principles calculations. Journal of Materials Science. **54**(1)493-505.
- Wang, H.-W., et al. (2016). Resolving the Structure of Ti3C2Tx MXenes through Multilevel Structural Modeling of the Atomic Pair Distribution Function. Chemistry of Materials. **28**(1)349-359.
- 20 31. Chu, Y.Z., et al. (2023). First-principles study of MXene properties with varying hydrofluoric acid concentration. iScience.
- 32. Kresse, G. and J. Furthmüller. (1996). Efficiency of ab-initio total energy calculations for metals and semiconductors using a plane-wave basis set. Computational Materials Science.
 6(1)15-50.
- 33. Kresse, G. and J. Furthmüller. (1996). Efficient iterative schemes for ab initio total-energy
 26 calculations using a plane-wave basis set. Physical Review B. 54(16)11169-11186.
- 34. Perdew, J.P., K. Burke, and M. Ernzerhof. (1996). Generalized Gradient Approximation
 Made Simple. Physical Review Letters. 77(18)3865-3868.
- 35. Grimme, S. (2006). *Semiempirical GGA-type density functional constructed with a long-range dispersion correction.* Journal of Computational Chemistry. **27**(15)1787-1799.
- 36. Momma, K. and F. Izumi. (2011). *VESTA 3 for three-dimensional visualization of crystal, volumetric and morphology data.* Journal of Applied Crystallography. **44**(6)1272-1276.
- 33 37. Tang, W., E. Sanville, and G. Henkelman. (2009). *A grid-based Bader analysis algorithm without lattice bias*. Journal of Physics: Condensed Matter. **21**(8)084204.
- 35 38. Yu, M. and D.R. Trinkle. (2011). Accurate and efficient algorithm for Bader charge integration. The Journal of chemical physics. **134**(6).